

# Geophysical Research Letters

## <del>L</del>

#### RESEARCH LETTER

10.1029/2023GL107181

#### **Key Points:**

- AMIP6 models remain plagued by large precipitation biases in the tropical Indo-Pacific region during summer with large inter-model spread
- This inter-model spread is dominated by an anomalous anticyclone (AAC) circulation over the northwest Pacific
- This AAC arises via barotropic energy conversion from mean circulation and is energized by convective feedbacks

#### **Supporting Information:**

Supporting Information may be found in the online version of this article.

#### Correspondence to:

H. Zhang, hzhang83@central.uh.edu; clarkzhang2009@gmail.com

#### Citation:

Zhang, H., Xie, S.-P., Seager, R., & Zhao, S. (2024). Dynamical constraint on precipitation biases over the Indo-Pacific region during boreal summer in AMIP6 models. *Geophysical Research Letters*, *51*, e2023GL107181. https://doi.org/10.1029/2023GL107181

Received 7 NOV 2023 Accepted 11 MAR 2024

#### **Author Contributions:**

Conceptualization: Honghai Zhang, Shang-Ping Xie Formal analysis: Honghai Zhang Funding acquisition: Honghai Zhang Investigation: Honghai Zhang, Siyu Zhao Methodology: Honghai Zhang, Shang-Ping Xie, Richard Seager Project administration: Honghai Zhang Supervision: Honghai Zhang, Shang-Ping Xie, Richard Seager Validation: Honghai Zhang Visualization: Honghai Zhang Writing - original draft: Honghai Zhang Writing - review & editing: Honghai Zhang, Shang-Ping Xie, Richard Seager, Siyu Zhao

#### © 2024. The Authors.

This is an open access article under the terms of the Creative Commons
Attribution-NonCommercial-NoDerivs
License, which permits use and distribution in any medium, provided the original work is properly cited, the use is non-commercial and no modifications or adaptations are made.

# **Dynamical Constraint on Precipitation Biases Over the Indo- Pacific Region During Boreal Summer in AMIP6 Models**

Honghai Zhang<sup>1,2</sup>, Shang-Ping Xie<sup>3</sup>, Richard Seager<sup>4</sup>, and Siyu Zhao<sup>1,2</sup>

<sup>1</sup>Department of Earth and Atmospheric Sciences, University of Houston, Houston, TX, USA, <sup>2</sup>Institute for Climate and Atmospheric Science, University of Houston, Houston, TX, USA, <sup>3</sup>Scripps Institution of Oceanography, University of California San Diego, La Jolla, CA, USA, <sup>4</sup>Lamont Doherty Earth Observatory, Columbia University, Palisades, NY, USA

**Abstract** Climate models suffer from longstanding precipitation biases, much of which has been attributed to their atmospheric component owing to unrealistic parameterizations. Here we investigate precipitation biases in 37 Atmospheric Model Intercomparison Project Phase 6 (AMIP6) models, focusing on the Indo-Pacific region during boreal summer. These models remain plagued by considerable precipitation biases, especially over regions of strong precipitation. In particular, 22 models overestimate the Asian-Pacific monsoon precipitation, while 28 models underestimate the southern Indian Ocean Intertropical Convergence Zone precipitation. The inter-model spread in summer precipitation is decomposed into Empirical Orthogonal Functions (EOFs). The leading EOF mode features an anomalous anticyclone circulation spanning the Indonorthwest Pacific oceans, which we show is energized by barotropic conversion from the confluence of the background monsoonal westerlies and trade-wind easterlies. Our results suggest precipitation biases in atmospheric models, though caused by unrealistic parameterizations, are organized by dynamical feedbacks of the mean flow.

Plain Language Summary The Indo-Pacific monsoonal rainfall provides life-supporting water to billions of people living in the region, and its associated latent heating drives changes in atmospheric circulation further affecting weather across the globe. The realistic simulation of rainfall over this important region remains challenging for generations of climate models. Many studies point to atmospheric models being the primary culprit, which motivates us to investigate the Indo-Pacific monsoonal rainfall simulated by the latest generation of atmospheric models in the sixth Atmospheric Model Intercomparison Project (AMIP6). We find that models examined here continue to struggle with, to various degree, simulating the observed distribution of Indo-Pacific monsoonal rainfall. We further find that variations in simulated rainfall among the AMIP6 models are not simply linked to their different model physics as previously thought, but are also strongly regulated by the atmospheric circulation over the Indo-northwest Pacific.

#### 1. Introduction

Climate models suffer from notorious longstanding precipitation biases, especially in the tropics (e.g., Bellucci et al., 2010; Mechoso et al., 1995; Neelin et al., 1992; Tian & Dong, 2020; Xiang et al., 2017). Precipitation biases in models degrade their simulation of weather and climate and render their future predictions and projections unreliable (e.g., Seager et al., 2019). Understanding and addressing these precipitation biases has been a goal for generations of climate scientists and modelers and will likely remain so for decades to come.

Precipitation biases in climate models arise from deficiencies in individual model components and their coupling. Take the tropics for example, fully coupled models share many similar precipitation biases with their uncoupled atmosphere/land-only simulations driven by observed ocean surface conditions, pointing to intrinsic deficiencies in the atmosphere/land models (e.g., Bellucci et al., 2010; Pathak et al., 2019; Xiang et al., 2017). However, fully coupled and uncoupled simulations also exhibit many different precipitation biases owing to their different (simulated vs. observed) ocean surface conditions, pointing to deficiencies in the ocean models (e.g., Richter, 2015) as well as in ocean-atmosphere coupling (e.g., Lin, 2007; Oueslati & Bellon, 2015; Z. Wang et al., 2018). In atmosphere/land models, one major intrinsic deficiency has been found in the parameterizations of atmospheric convection, where parameters that have been identified critical for precipitation biases include convection closure (Pathak et al., 2019; G. J. Zhang & Wang, 2006), convection triggers (Bellucci et al., 2010; Oueslati & Bellon, 2015) and lateral entrainment (Hirota et al., 2011). In fully coupled models, precipitation

ZHANG ET AL. 1 of 10

biases are often linked tightly with biases in sea surface temperature (SST), which can be caused by underrepresented atmospheric processes such as clouds (e.g., Hwang & Frierson, 2013; Li & Xie, 2013), underrepresented oceanic processes such as coastal upwelling and meso-to-small scale mixing (e.g., Richter, 2015) as well as unrealistic coupled ocean-atmosphere feedbacks (e.g., Lin, 2007). Quantifying these sources of precipitation/SST biases in fully coupled models has proven extremely difficult owing to the complex nature of coupling and potential compensation of errors in individual model components.

However, prior research based on the Coupled Model Intercomparison Project (CMIP) phases 3, 5 and 6 has appeared to come to a consensus that precipitation biases in the tropics (except certain regions) likely arise mostly from the atmosphere/land models. This consensus is based on the findings that many of the tropical precipitation biases in the fully coupled models are also present in their atmosphere/land-only components. In particular, Xiang et al. (2017) have analyzed the double Intertropical Convergence Zone (ITCZ) problem in the CMIP5 archive—a persistent issue (also in CMIP3 and 6 (Tian & Dong, 2020)) featuring excessive precipitation in the southern-hemisphere tropics than observed. Xiang et al. have shown that the double ITCZ problem in the CMIP5 coupled models is tightly linked with the tropical SST biases (consistent with prior research); more importantly, these tropical SST biases in the coupled models are further attributed to the biases in the tropical ocean surface heat flux in the corresponding atmosphere/land-only simulations (driven by observed SSTs). As a result, the double ITCZ problem in fully coupled models can be well predicted by the surface heat flux biases intrinsic in the corresponding atmosphere/land-only models (which will induce SST biases when coupled) with a prediction skill (i.e., correlation) up to 0.9. These findings by Xiang et al., and many others, suggest that the largest source of the tropical precipitation biases in coupled climate models lies in the intrinsic deficiencies in the atmosphere/land models in the tropics.

Motivated by the above prior research, here we aim to investigate precipitation biases in the atmosphere/land-only simulations driven by observed SSTs and sea ice concentrations from the sixth Atmospheric Model Intercomparison Project (AMIP6) (Eyring et al., 2016). We focus on the boreal summer season June to August (JJA) over the broad Indo-Pacific region (30°N–25°S, 30°E–150°E) covering south/southeast Asia—the most densely populated area on Earth and the southern Indian Ocean—an area where precipitation biases are much less studied than in the tropical Pacific and Atlantic Oceans. Specifically, we address two questions: (a) how well do AMIP6 models simulate the JJA mean precipitation over the Indo-Pacific region? (b) what controls the inter-model spread of precipitation biases across these models in the region? To address these questions, we will evaluate AMIP6 models against observations and conduct statistical analyses including Empirical Orthogonal Function (EOF) decomposition, explained further next.

#### 2. Data and Methodology

For observed precipitation, we use two different products to account for observational uncertainties (due to random and systematic errors in raw observations and various algorithms to merge those observations). These include the CPC Merged Analysis of Precipitation (CMAP) standard product (P. Xie & Arkin, 1997) and the Global Precipitation Climatology Project (GPCP) version 2.3 (Adler et al., 2018). Both CMAP and GPCP are a blend of satellite and gauge data sets but differ in terms of satellite sensors and blending algorithms (Adler et al., 2018; P. Xie & Arkin, 1997). Over the study area (30°N–25°S, 30°E–150°E), CMAP exhibits stronger annual mean precipitation rates than GPCP (not shown). Their long-term monthly climatology from 1981 to 2010 at 2.5° resolution is used to evaluate model simulations.

We analyze the atmosphere/land-only simulations from 37 models in the AMIP6 archive (Table S1 in Supporting Information S1). Since all these simulations are driven by the same observed SST and sea ice conditions and radiative forcing, their performance in simulating precipitation can be attributed to the atmosphere/land dynamics and physics. All model data and observations are interpolated onto the same 1° by 1° grid to allow quantitative comparison.

To investigate the differences among the AMIP6 models, we conduct the EOF decomposition of the inter-model variance across the 37 models. EOF is typically applied to extract the variability with large spatiotemporal variance (i.e., in the time domain), but it has also been used to isolate the main processes that cause the intermodel spread across CMIP models (e.g., Li & Xie, 2013). Here we apply the inter-model EOF analysis to examine the leading processes responsible for the different performance of the AMIP6 models in simulating the summer precipitation climatology over the study area (30°N–25°S, 30°E–150°E).

ZHANG ET AL. 2 of 10

19448007, 2024, 6, Downloaded from https://agupubs.onlinelibrary.wiley.com/doi/10.10292023GL107181 by University Of Houston Library, Wiley Online Library on [30/01/2025]. See the Terms

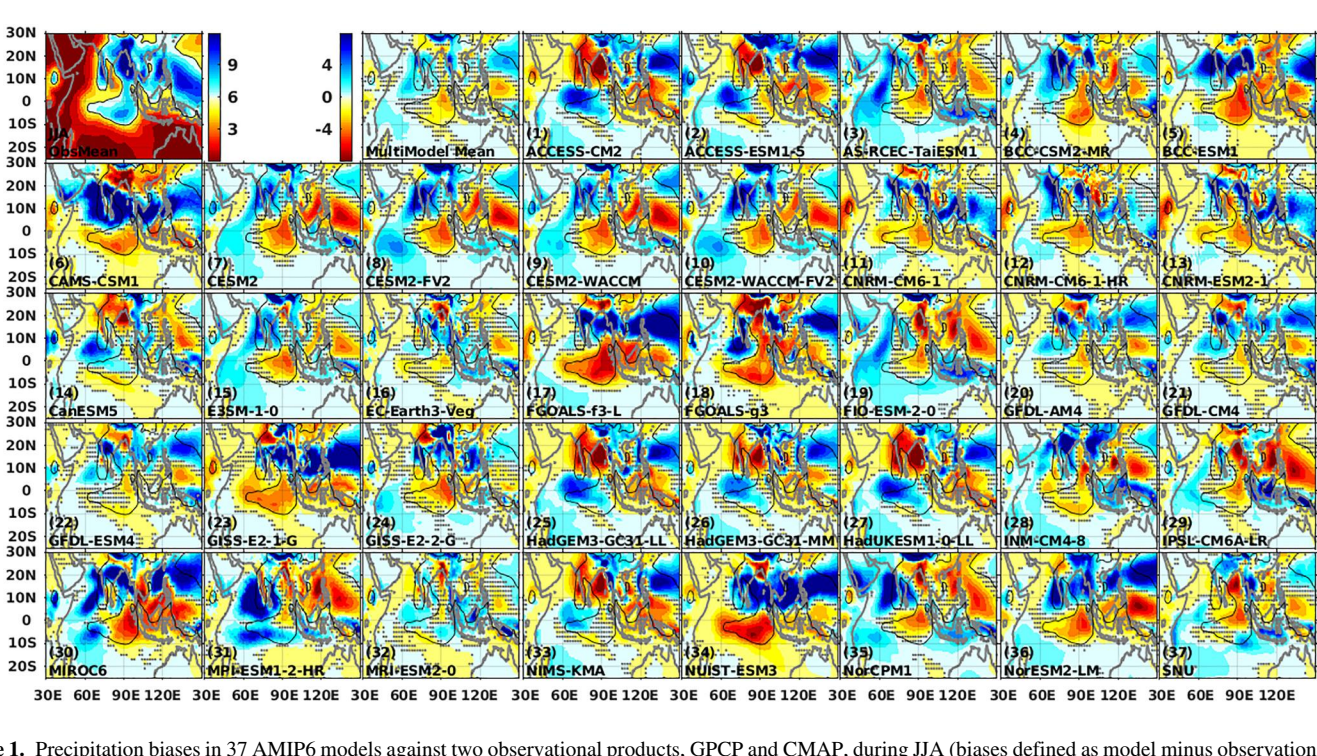


**Figure 1.** Precipitation biases in 37 AMIP6 models against two observational products, GPCP and CMAP, during JJA (biases defined as model minus observation). Top left panel shows the average precipitation rate (mm/day) between GPCP and CMAP, while the remaining panels show biases of each individual model as well as the multi-model mean (labeled in the lower left corner of each panel). The color scale for observed precipitation is 0–12 mm/day and for model biases is –8 mm/day to 8 mm/day. As a reference, the observed 6 mm/day precipitation rate is plotted in black contour in all panels. Gray stippling as a measure of significance indicates that the model precipitation is within the range defined by GPCP and CMAP (i.e., the observational uncertainty).

#### 3. Results

Over the study area (30°N–25°S, 30°E–150°E) during JJA, high precipitation rates (e.g., >6 mm/day) are observed over the south Asia monsoon and the Inter-tropical Convergence Zone (ITCZ) from the tropical northwest Pacific to the southern Indian Ocean (Figure 1). As in prior generations of AMIP simulations, this observed spatial distribution is mostly reproduced by the AMIP6 models examined here, but all these current-generation models still suffer from significant biases in the magnitude of precipitation rates (Figure 1). Notably, strong biases tend to occur in regions of high precipitation rates. Over the south Asia monsoon region, the AMIP6 multi-model mean overestimates observed precipitation (a similar bias has been identified in AMIP5 by Wang et al., 2018), but individual models show a large spread of biases, with several models severely underestimating the monsoonal precipitation (e.g., ACCESS-CM2, ACCESS-ESM1-5, HadGEM3-GC31-LL/-MM, HadUKESM1-0, as most of the fully coupled CMIP models (e.g., He et al., 2023)). Similarly, the tropical northwest Pacific also exhibits a multi-model mean of relatively weak overestimation that results from large compensating biases in individual models. Over the southern Indian Ocean ITCZ, most of the AMIP6 models and the multi-model mean underestimate the ITCZ precipitation.

To quantify the distribution of precipitation biases across the AMIP6 models, we select three regions where observed mean precipitation rate is higher than 6 mm/day and compute the areal mean bias (Figure 2). The first region is over the southern Indian Ocean ITCZ (0°N–20°S, 50°E–110°E), an intriguing ITCZ that has received little attention in literature (e.g., Zhang et al., 2022). All 37 AMIP6 models are able to simulate the local rainfall maximum associated with this ITCZ (not shown), but three quarters (28) of the models underestimate its precipitation during JJA. The second and third regions cover the south Asian monsoon (25°N–0°S, 40°E–100°E) and the tropical northwest Pacific ITCZ (25°N–0°S, 100°E–140°E), respectively. Again, all AMIP6 models successfully simulate the associated precipitation local maxima, but large spread exists across individual models with 22 models overestimating the observed precipitation in each of these two regions, respectively (Figure 2).

To investigate the spread among the AMIP6 models, we conduct EOF decomposition of the inter-model variance of the JJA mean precipitation over the region of large precipitation spread across models  $(25^{\circ}N-10^{\circ}S, 40^{\circ}E-140^{\circ})$ 

ZHANG ET AL. 3 of 10

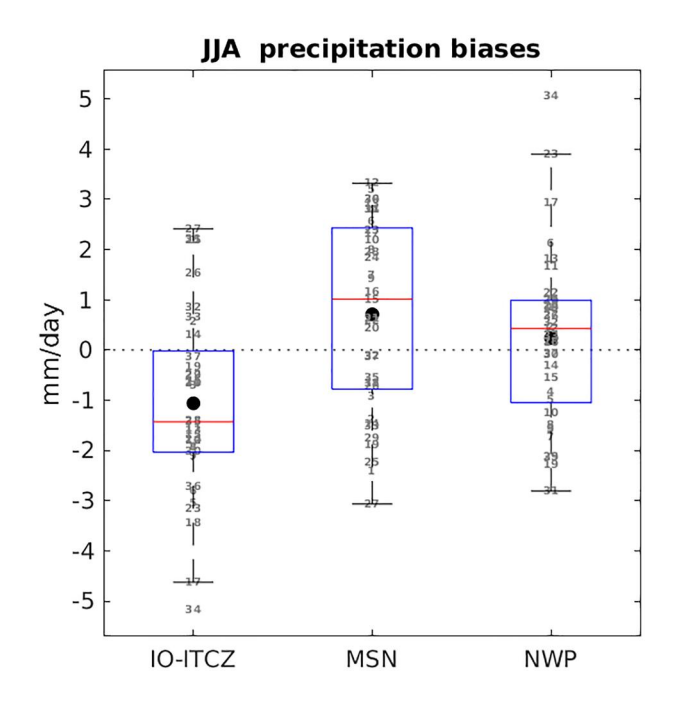


**Figure 2.** Box-whisker plot of JJA precipitation biases of the 37 AMIP6 models averaged over three selected regions, the southern Indian Ocean ITCZ (IO-ITCZ, 0°N–20°S, 50°E–110°E), the south Asian Monsoon (MSN, 25°N–0°S, 40°E–100°E) and the Northwest Pacific (NWP, 25°N–0° S, 100°E–140°E). The domain average is calculated only for regions where observed mean precipitation rate is higher than 6 mm/day. On each box, the central red mark indicates the median, and the bottom and top blue edges indicate the 25th and 75th percentiles, respectively. The whiskers extend to values that are within 1.5 times the distance between the 25th and 75th percentiles from these percentiles. The numbers in gray are individual AMIP6 models numbered in Figure 1 (within the parentheses in the lower left corner of each panel above the model's name).

E). The top two EOF modes explain similar amounts of variance, 25.3% and 23.1%, respectively, and are significantly (North et al., 1982) separated from all other EOF modes but not from each other (Figure 3c). The first EOF mode (Figure 3a) features a meridional dipole of precipitation anomalies between about 50°E and 150°E over two zonal bands, the south Asia-northwest tropical Pacific band and the tropical Indian Ocean-maritime continents band. This precipitation pattern is associated with large-scale anomalous winter monsoon-like winds over south Asia and anomalous anticyclonic winds over the northwest Pacific. The second EOF mode features a quadruple pattern of precipitation anomalies with centers-of-action over the Indian subcontinent, the tropical Indian Ocean, the maritime continents and the tropical northwest Pacific east of Philippines, respectively. This quadruple precipitation pattern is also associated with consistent wind anomalies, with anticyclonic winds over reduced precipitation and cyclonic winds over enhanced precipitation. These two EOF modes are actually quite visible even in the raw precipitation biases in Figure 1. For example, the first EOF mode can be seen in FGOALS-f3-L, the three GFDL models (#20-22), GISS-E2-1-G, MIROC6, NUIST-ESM3 and NorESM2-LM, while the second EOF mode is visible in the two ACCESS models (#1-2), the three Hadley models (#25-27), NIMS-KMA and NorCPM1 (with opposite polarity). These results confirm that the top two EOF modes, although being inseparable with similar amounts of explained variance, indeed capture the dominant patterns of the spread in the summer precipitation climatology across the AMIP6 models.

These two EOF modes are nearly identical to those associated with the anomalous anticyclone (AAC) mode in Wang et al. (2021, cf., Figures 2a and 2b therein). The AAC is an intrinsic mode of atmospheric variability over the tropical northwest Pacific during boreal summer across the intraseasonal to interannual time scales with marked impacts on the Asian-Pacific monsoon (Box 11.1 of S.-P. Xie (2023)). It arises from the confluence of the monsoonal westerlies over the northern Indian Ocean and the trade wind easterlies over the western tropical Pacific. The kinetic energy associated with this climatological confluence is the fundamental source of energy that drives the AAC

via barotropic energy conversion, and the AAC is further energized by moist circulation-convection positive feedbacks and sustained by local air-sea coupling (Song & Zhou, 2014). On the intraseasonal time scale, the AAC manifests itself as variability that propagates both eastward and northward, akin to the Madden-Julian Oscillation (see Figure 4 in Wang et al., 2021). On the interannual time scale, the AAC appears as a stationary mode over the northwest Pacific and can be triggered by other interannual variability, especially El Niño.

The similarity between our top two EOF modes and those in Wang et al. (2021) is rather surprising given that the EOF modes associated with the AAC are derived from the covariance of 20-day low-pass filtered daily horizontal winds at 850 and 200 hPa in observation-based reanalysis, as opposed to our EOF analysis of the variance of seasonal precipitation climatology across the AMIP6 models. (We adopted the same region of Wang et al. for the EOF analysis.). Note that the EOF pairs are not only similar in terms of the spatial pattern, but also regarding the variance explained—both EOF pairs have statistically inseparable eigenvalues explaining similar amount of the corresponding total analyzed variance, 25.3% and 23.1% for our EOF pair compared with 15.4% and 12.6% for the EOF pair associated with the AAC. In the time-domain, this EOF pair represents two different phases of the AAC propagating in space; however in the model domain, our EOF pair does not imply propagation across models but likely suggests that precipitation biases in different models are dominated by different phases of the AAC. These surprising similarities are unlikely a coincidence but suggest an important role of the AAC dynamics in regulating the spread of summer precipitation climatology across the AMIP6 models over the Indo-Pacific region.

To provide support for this assertion, we calculate the barotropic energy conversion—the fundamental driver of the AAC—in an inter-model manner similar to our EOF analysis above. Specifically, the "barotropic energy conversion" (see derivation in Appendix A) is calculated by

ZHANG ET AL. 4 of 10



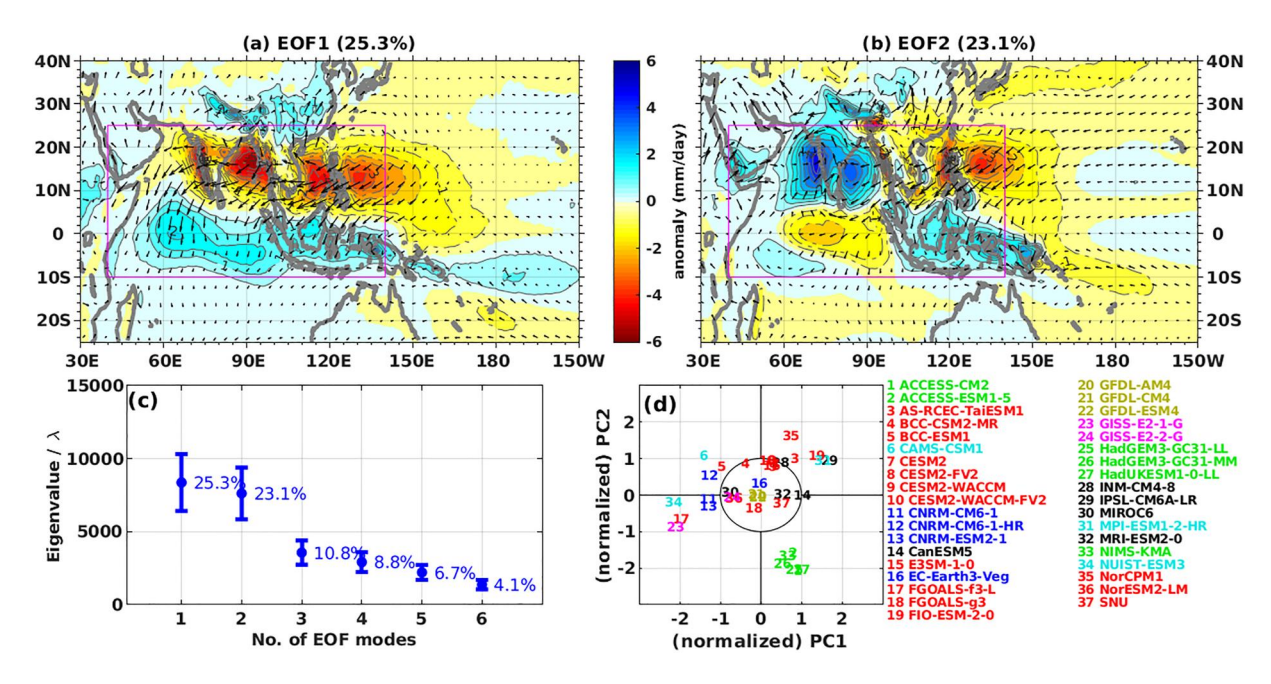


Figure 3. EOF decomposition of the inter-model variance of JJA mean precipitation across the 37 AMIP6 models over the region indicated by the magenta box in (a), (b) (25°N-10°S, 40°E-140°E). (a) and (b): the first and second EOF mode, respectively, showing the regressed departures of precipitation (shading, mm/day) and 925 hPa wind (vectors, m/s) from the multi-model mean against the normalized principal components (PC) of the EOF modes. (c) The eigenvalues of the top six EOF modes. (d) The distribution of the 37 AMIP6 models as a function of the normalized PCs of the top two EOFs. Models sharing similar atmosphere components are grouped in colors, except black (Kuma et al., 2023).

$$\overline{BTC} = -\left(\overline{u'^2}\frac{\partial \overline{u}}{\partial x} + \overline{v'^2}\frac{\partial \overline{v}}{\partial y}\right) - \overline{u'v'}\left(\frac{\partial \overline{u}}{\partial y} + \frac{\partial \overline{v}}{\partial x}\right)$$

where u, v are the zonal and meridional winds at 925 hPa, and overbar and prime denote the multi-model ensemble mean and the departure of the individual model from the ensemble mean, respectively (in the same manner as the inter-model EOF analysis). Here the quotes on "barotropic energy conversion" emphasize that the computation is done in the model domain as opposed to the time domain. Nonetheless, the BTC contributes to the inter-model spread of circulation in the same way as the barotropic instability in the time domain (i.e., transient eddies grow by extracting energy from the time-mean flow). The multi-model mean  $\overline{BTC}$  (Figure 4a) shows positive "barotropic energy conversion" over the confluence region in the northwest Pacific between about 10°N and 20° N. Further decomposition of this quantity (Figures 4b-4e) confirms that the positive contributions arise mostly from the confluence of monsoonal westerlies and trade wind easterlies (i.e.,  $\frac{\partial \overline{u}}{\partial x}$ ). Figure 4b) and secondarily from the meridional shear of zonal mean winds (i.e.,  $\frac{\partial \overline{u}}{\partial v}$ , Figure 4d) over the northwest Pacific. These results are consistent with the time-domain diagnostics in Wang et al. (2021, cf. Figure 8a therein), thus lending processlevel support to the assertion that the AAC, as a dynamical mode, plays an important role in regulating the inter-model spread of summer precipitation climatology across the AMIP6 models over the Indo-Pacific region.

These results could be understood in terms of the strong precipitation-circulation coupling in the tropics. On the one hand, in observations the AAC is a least-damped mode of circulation variability in the Indo-Pacific region owing to barotropic instability (e.g., Simmons et al., 1983) associated with the horizontal shear of the mean flow. On the other hand, global climate models including the AMIP6 models are able to simulate the salient features of the mean flow in the Indo-Pacific region (e.g., the monsoonal westerlies-trade wind easterlies confluence, albeit with varying degrees of realism), suggesting that models are very likely able to simulate the observed fundamental dynamics such as barotropic instability. Given the strong precipitation-circulation coupling, precipitation biases induced by deficiencies in relevant parameterizations will cause circulation biases. Although these circulation biases differ markedly across models (depending on model parameterizations), they (like an imposed external forcing) could trigger the least-damped mode of circulation variability in the Indo-Pacific region—the

ZHANG ET AL. 5 of 10

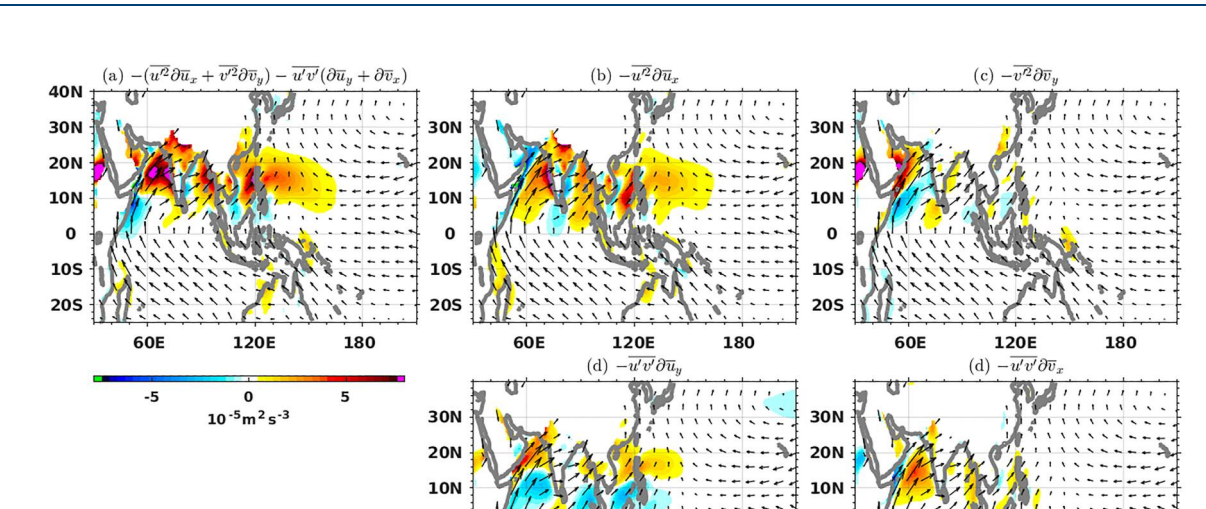


**Figure 4.** Estimation of the "barotropic energy conversion" (shading) across the AMIP6 models (a) and its decomposition into components associated with  $\frac{\partial \overline{u}}{\partial x}$  (b),  $\frac{\partial \overline{v}}{\partial y}$  (c),  $\frac{\partial \overline{u}}{\partial y}$  (d) and  $\frac{\partial \overline{v}}{\partial x}$  (e), respectively. 925 hPa winds are used in this estimation (to be consistent with the EOF analysis in Figure 3); vectors denote the multi-model mean 925 hPa winds. Details of the estimation are explained in the main text and Appendix A. Results using 850 hPa winds as in Wang et al. (2021) are similar (not shown).

120E

AAC—via barotropic instability in all models. This common dynamical response will feedback onto and reorganize the precipitation biases originally induced by parameterization deficiencies, such that these precipitation biases eventually take on the spatial structure of the AAC—likely different phases of the AAC in different models. Therefore, the leading EOF modes of the inter-model spread of the precipitation biases emerge as the AAC.

0

105

205

120E

180

180

#### 4. Summary and Discussions

0

205

This work is motivated by prior findings in the literature that the longstanding precipitation biases in fully coupled models could arise from their atmosphere components and hence the premise that understanding precipitation biases in atmospheric models will help improve the development of fully coupled models. Here we first evaluate the performance of 37 AMIP6 models in simulating the precipitation climatology over the region covering the Asian-Pacific monsoon and the southern Indian Ocean (30°N–25°S, 30°E–150°E) during boreal summer and then investigate the causes of the varying performances across the models.

The 37 AMIP6 models driven by observed boundary conditions are mostly able to simulate the spatial pattern of observed summer precipitation climatology, especially the strong precipitation over the monsoon and ITCZ regions. However, all of these AMIP6 models still suffer from significant biases in the magnitude of precipitation rates. Large biases tend to occur over regions of strong precipitation rates. Specifically, most of the AMIP6 models struggle to simulate the full strength of the southern Indian Ocean ITCZ, with 28 out of the 37 models significantly underestimating the ITCZ precipitation. Over the Asian-Pacific monsoon region, the AMIP6 multimodel mean slightly overestimates observed precipitation, but individual models have a wide spread of biases with some models significantly underestimating the monsoonal precipitation.

Applying the inter-model EOF analysis, we find that the spread of summer precipitation climatology across the AMIP6 models is dominated by the Anomalous Anticyclone mode over the northwest Pacific. The AAC is an intrinsic mode of circulation variability on intraseasonal to interannual time scales, owes its existence essentially to the confluence of monsoonal westerlies over the northern Indian Ocean and trade wind easterlies over the western Pacific via barotropic energy conversion and is further energized by positive feedbacks between circulation and moist convection. The barotropic energy conversion evaluated across the AMIP6 models (in a way analogous to the inter-model EOF analysis) shows strong positive values over the northwest Pacific where monsoonal westerlies and trade wind easterlies converge, which supports the argument that the leading patterns of

ZHANG ET AL. 6 of 10

summer mean precipitation spread across the AMIP6 models over the Indo-Pacific region are a reflection of the AAC. These new findings suggest that precipitation biases in the AMIP6 models, caused originally by deficiencies in the atmosphere/land parameterizations, are strongly regulated by intrinsic atmospheric dynamics (to the extent that these dynamics are realistically simulated).

Based on analysis of the inter-model spread in CMIP3 fully coupled models, Kosaka and Nakamura (2011) found that the biases in mean summer precipitation over the western North Pacific are regulated by the so-called Pacific-Japan teleconnection pattern, which features the AAC pattern in the tropics and originates from intrinsic atmospheric dynamics. Kosaka and Nakamura further speculated that the regulation of precipitation biases by the Pacific-Japan pattern is triggered by remote SST biases over the tropical Pacific and Indian Ocean. However, our results based on the AMIP6 simulations, which by design have no SST biases, suggest that the strong dynamical regulation of precipitation biases by atmospheric circulation variability such as the AAC does not require external triggers like SST biases, but rather is an intrinsic process in the atmosphere/land models. Our work highlights a dynamical constraint on precipitation biases by atmospheric circulation and provides process-level insights for improving fully coupled climate models, a task we are undertaking.

#### **Appendix: Derivation of Barotropic Energy Conversion**

Since we are concerned with barotropic instability, we ignore the vertical motion and only consider the case of horizontal flows. The horizontal momentum equations may be written as

$$\left(\frac{\partial}{\partial t} + u \frac{\partial}{\partial x} + v \frac{\partial}{\partial y}\right) u = F_x$$

$$\left(\frac{\partial}{\partial t} + u\frac{\partial}{\partial x} + v\frac{\partial}{\partial y}\right)v = F_y$$

where u,v are zonal and meridional winds and  $F_x,F_y$  are zonal and meridional components of net horizontal forces (including Coriolis force, pressure gradient force and viscous force). Linearization of momentum equations is typically done in time domain—by decomposing a field into a temporal average and a deviation from the temporal average, for example,  $u = \overline{u} + u'$ , where bar and prime denote temporal average and transient deviation, respectively. However, here we linearize the equations about the multi-model mean, with bar and prime denoting multi-model mean and model deviation from the multi-model mean, respectively. Assuming deviations are small, we derive the following linearized momentum equations (identical to those in time domain)

$$\left(\frac{\partial}{\partial t} + \overline{u}\frac{\partial}{\partial x} + \overline{v}\frac{\partial}{\partial y}\right)u' + u'\frac{\partial\overline{u}}{\partial x} + v'\frac{\partial\overline{u}}{\partial y} = \overline{F}_x + F_x'$$

$$\left(\frac{\partial}{\partial t} + \overline{u}\frac{\partial}{\partial x} + \overline{v}\frac{\partial}{\partial y}\right)v' + u'\frac{\partial\overline{v}}{\partial x} + v'\frac{\partial\overline{v}}{\partial y} = \overline{F}_y + F_y'$$

Multiplying u',v' to the above equations, respectively, summing them up and moving the anomalous advection terms to the rhs yield the kinetic energy  $\left(KE \equiv \frac{u'^2 + v'^2}{2}\right)$  equation,

$$\left(\frac{\partial}{\partial t} + \overline{u}\frac{\partial}{\partial x} + \overline{v}\frac{\partial}{\partial y}\right) KE = -\left[u'^{2}\frac{\partial \overline{u}}{\partial x} + v'^{2}\frac{\partial \overline{v}}{\partial y} + u'v'\left(\frac{\partial \overline{u}}{\partial y} + \frac{\partial \overline{v}}{\partial x}\right)\right] + u'\left(\overline{F}_{x} + F_{x}'\right) + v'\left(\overline{F}_{y} + F_{y}'\right).$$

If we further apply the quasi-geostrophic approximation to the multi-model mean flow,  $\frac{\partial \overline{u}}{\partial x} + \frac{\partial \overline{v}}{\partial y} \approx 0$ , the first term on the rhs can be rewritten as

$$-\left[u'^{2}\frac{\partial \overline{u}}{\partial x}+v'^{2}\frac{\partial \overline{v}}{\partial y}+u'v'\left(\frac{\partial \overline{u}}{\partial y}+\frac{\partial \overline{v}}{\partial x}\right)\right]\approx-\left[\left(u'^{2}-v'^{2}\right)\frac{\partial \overline{u}}{\partial x}+u'v'\left(\frac{\partial \overline{u}}{\partial y}+\frac{\partial \overline{v}}{\partial x}\right)\right]$$

ZHANG ET AL. 7 of 10

Acknowledgments

## **Geophysical Research Letters**

which has the same form as the barotropic energy conversion used in the time domain in literature (Hoskins et al., 1983; Simmons et al., 1983).

By analogy, we define BTC  $\equiv -\left[u'^2\frac{\partial\overline{u}}{\partial x} + v'^2\frac{\partial\overline{v}}{\partial y} + u'v'\left(\frac{\partial\overline{u}}{\partial y} + \frac{\partial\overline{v}}{\partial x}\right)\right]$  as the "barotropic energy conversion" in the model domain; note that the quasi-geostrophic approximation is not assumed. Based on the KE equation, BTC contributes to the inter-model spread of model flow in a way analogous to the barotropic instability in the time domain.

#### **Data Availability Statement**

This work utilizes 37 AMIP6 simulations (see Supporting Information S1) that are freely available from the Earth System Grid Federation (https://esgf-node.llnl.gov/search/cmip6/) and two observation-based precipitation data sets, CMAP (P. Xie & Arkin, 1997) and GPCC (Adler et al., 2018), freely available at the NOAA PSL, Boulder, Colorado, USA (https://psl.noaa.gov).

#### References

This work is funded by the NSF awards AGS 1934363, 1934392, 2101214, and 231170. Constructive comments from anonymous reviewers are appreciated.

Adler, R. F., Sapiano, M. R. P., Huffman, G. J., Wang, J.-J., Gu, G., Bolvin, D., et al. (2018). The global precipitation climatology project (GPCP) monthly analysis (new version 2.3) and a review of 2017 global precipitation [Dataset]. Atmosphere, 9(4), 138. https://doi.org/10.3390/atmos9040138

Bellucci, A., Gualdi, S., & Navarra, A. (2010). The double-ITCZ syndrome in coupled general circulation models: The role of large-scale vertical circulation Regimes. *Journal of Climate*, 23(5), 1127–1145. https://doi.org/10.1175/2009JCLI3002.1

Eyring, V., Bony, S., Meehl, G. A., Senior, C. A., Stevens, B., Stouffer, R. J., & Taylor, K. E. (2016). Overview of the coupled model inter-comparison project phase 6 (CMIP6) experimental design and organization. *Geoscientific Model Development*, 9(5), 1937–1958. https://doi.org/10.5194/gmd-9-1937-2016

He, L., Zhou, T., & Chen, X. (2023). South Asian summer rainfall from CMIP3 to CMIP6 models: Biases and improvements. *Climate Dynamics*, 61(3), 1049–1061. https://doi.org/10.1007/s00382-022-06542-4

Hirota, N., Takayabu, Y. N., Watanabe, M., & Kimoto, M. (2011). Precipitation reproducibility over tropical oceans and its relationship to the double ITCZ problem in CMIP3 and MIROC5 climate models. *Journal of Climate*, 24(18), 4859–4873. https://doi.org/10.1175/ 2011ICI.14156.1

Hoskins, B. J., James, I. N., & White, G. H. (1983). The Shape, propagation and mean-flow interaction of large-scale weather systems. *Journal of the Atmospheric Sciences*, 40(7), 1595–1612. https://doi.org/10.1175/1520-0469(1983)040<1595:TSPAMF>2.0.CO;2

Hwang, Y.-T., & Frierson, D. M. W. (2013). Link between the double-intertropical convergence zone problem and cloud biases over the Southern Ocean. *Proceedings of the National Academy of Sciences of the United States of America*, 110(13), 4935–4940. https://doi.org/10.1073/pnas.

Kosaka, Y., & Nakamura, H. (2011). Dominant mode of climate variability, intermodel diversity, and projected future changes over the summertime Western North Pacific simulated in the CMIP3 models. *Journal of Climate*, 24(15), 3935–3955. https://doi.org/10.1175/2011JCLI3907.1

Kuma, P., Bender, F. A.-M., & Jönsson, A. R. (2023). Climate model code genealogy and its relation to climate feedbacks and sensitivity. *Journal of Advances in Modeling Earth Systems*, 15(7), e2022MS003588. https://doi.org/10.1029/2022MS003588

Li, G., & Xie, S.-P. (2013). Tropical biases in CMIP5 multimodel ensemble: The excessive equatorial Pacific cold tongue and double ITCZ problems. *Journal of Climate*, 27(4), 1765–1780. https://doi.org/10.1175/JCLI-D-13-00337.1

Lin, J.-L. (2007). The double-ITCZ problem in IPCC AR4 coupled GCMs: Ocean–atmosphere feedback analysis. *Journal of Climate*, 20(18), 4497–4525. https://doi.org/10.1175/JCL14272.1

Mechoso, C. R., Robertson, A. W., Barth, N., Davey, M. K., Delecluse, P., Gent, P. R., et al. (1995). The seasonal cycle over the tropical Pacific in coupled ocean–atmosphere general circulation models. *Monthly Weather Review*, 123(9), 2825–2838. https://doi.org/10.1175/1520-0493 (1995)123<2825:TSCOTT>2.0.CO:2

Neelin, J. D., Latif, M., Allaart, M. A. F., Cane, M. A., Cubasch, U., Gates, W. L., et al. (1992). Tropical air-sea interaction in general circulation models. Climate Dynamics, 7(2), 73–104. https://doi.org/10.1007/BF00209610

North, G. R., Bell, T. L., Cahalan, R. F., & Moeng, F. J. (1982). Sampling errors in the estimation of empirical orthogonal functions. *Monthly Weather Review*, 110(7), 699–706. https://doi.org/10.1175/1520-0493(1982)110<0699:SEITEO>2.0.CO;2

Oueslati, B., & Bellon, G. (2015). The double ITCZ bias in CMIP5 models: Interaction between SST, large-scale circulation and precipitation. Climate Dynamics, 44(3), 585–607. https://doi.org/10.1007/s00382-015-2468-6

Pathak, R., Sahany, S., Mishra, S. K., & Dash, S. K. (2019). Precipitation biases in CMIP5 models over the South Asian region. *Scientific Reports*, 9(1), 9589. https://doi.org/10.1038/s41598-019-45907-4

Richter, I. (2015). Climate model biases in the eastern tropical oceans: Causes, impacts and ways forward. WIREs Climate Change, 6(3), 345–358. https://doi.org/10.1002/wcc.338

Seager, R., Cane, M., Henderson, N., Lee, D.-E., Abernathey, R., & Zhang, H. (2019). Strengthening tropical Pacific zonal sea surface temperature

gradient consistent with rising greenhouse gases. *Nature Climate Change*, 9(7), 517–522. https://doi.org/10.1038/s41558-019-0505-x Simmons, A. J., Wallace, J. M., & Branstator, G. W. (1983). Barotropic wave propagation and instability, and atmospheric teleconnection patterns. *Journal of the Atmospheric Sciences*, 40(6), 1363–1392. https://doi.org/10.1175/1520-0469(1983)040<1363:BWPAIA>2.0.CO;2

Song, F., & Zhou, T. (2014). The climatology and interannual variability of east Asian summer monsoon in CMIP5 coupled models: Does air–sea coupling improve the simulations? *Journal of Climate*, 27(23), 8761–8777. https://doi.org/10.1175/JCLI-D-14-00396.1

Tian, B., & Dong, X. (2020). The double-ITCZ bias in CMIP3, CMIP5, and CMIP6 models based on annual mean precipitation. *Geophysical Research Letters*, 47(8), e2020GL087232. https://doi.org/10.1029/2020GL087232

Wang, X., Xie, S.-P., Guan, Z., & Wang, M. (2021). A common base mode of Asian summer monsoon variability across timescales. *Journal of Climate*, 34(18), 7359–7371. https://doi.org/10.1175/JCLI-D-20-0856.1

ZHANG ET AL. 8 of 10



## **Geophysical Research Letters**

- 10.1029/2023GL107181
- Wang, Z., Li, G., & Yang, S. (2018). Origin of Indian summer monsoon rainfall biases in CMIP5 multimodel ensemble. *Climate Dynamics*, 51(1), 755–768, https://doi.org/10.1007/s00382-017-3953-x
- Xiang, B., Zhao, M., Held, I. M., & Golaz, J.-C. (2017). Predicting the severity of spurious "double ITCZ" problem in CMIP5 coupled models from AMIP simulations. *Geophysical Research Letters*, 44(3), 1520–1527. https://doi.org/10.1002/2016GL071992
- Xie, P., & Arkin, P. A. (1997). Global precipitation: A 17-year monthly analysis based on gauge observations, satellite estimates, and numerical model outputs [Dataset]. Bulletin of the American Meteorological Society, 78(11), 2539–2558. https://doi.org/10.1175/1520-0477(1997) 078<2539:GPAYMA>2.0.CO:2
- Xie, S.-P. (2023). Coupled atmosphere-ocean dynamics: From El Niño to climate change (p. 424). Elsevier. https://doi.org/10.1016/c2021-0-02107-6
- Zhang, G. J., & Wang, H. (2006). Toward mitigating the double ITCZ problem in NCAR CCSM3. Geophysical Research Letters, 33(6). https://doi.org/10.1029/2005GL025229
- Zhang, H., Seager, R., & Xie, S.-P. (2022). How does sea surface temperature drive the intertropical convergence zone in the southern Indian Ocean? *Journal of Climate*, 35(16), 5415–5432. https://doi.org/10.1175/JCLI-D-21-0870.1

#### **References From the Supporting Information**

- Bader, D. C., Leung, R., Taylor, M., & McCoy, R. B. (2019). E3SM-Project E3SM1.0 model output prepared for CMIP6 CMIP [Dataset]. Earth System Grid Federation. https://doi.org/10.22033/ESGF/CMIP6.2294
- Bethke, I., Wang, Y., Counillon, F., Kimmritz, M., Fransner, F., Samuelsen, A., et al. (2019). NCC NorCPM1 model output prepared for CMIP6 CMIP AMIP [Dataset]. Earth System Grid Federation. https://doi.org/10.22033/ESGF/CMIP6.10863
- Boucher, O., Denvil, S., Levavasseur, G., Cozic, A., Caubel, A., Foujols, M.-A., et al. (2018). IPSL IPSL-CM6A-LR model output prepared for CMIP6 CMIP AMIP [Dataset]. Earth System Grid Federation. https://doi.org/10.22033/ESGF/CMIP6.5113
- Byun, Y.-H., Lim, Y.-J., Sung, H. M., Kim, J., Sun, M., & Kim, B.-H. (2019). NIMS-KMA KACE1.0-G model output prepared for CMIP6 CMIP AMIP [Dataset]. Earth System Grid Federation. https://doi.org/10.22033/ESGF/CMIP6.8350
- Cao, J., & Wang, B. (2019). NUIST NESMv3 model output prepared for CMIP6 CMIP [Dataset]. Earth System Grid Federation. https://doi.org/10.22033/ESGF/CMIP6.2021
- Cole, J. N. S., von Salzen, K., Swart, N. C., Kharin, V. V., Lazare, M., Scinocca, J. F., et al. (2019). CCCma CanESM5 model output prepared for CMIP6 CFMIP amip-p4K [Dataset]. Earth System Grid Federation. https://doi.org/10.22033/ESGF/CMIP6.3548
- Danabasoglu, G. (2019a). NCAR CESM2 model output prepared for CMIP6 CMIP AMIP [Dataset]. Earth System Grid Federation. https://doi.
- org/10.22033/ESGF/CMIP6.7522
  Danabasoglu, G. (2019b). NCAR CESM2-WACCM model output prepared for CMIP6 CMIP AMIP [Dataset]. Earth System Grid Federation.
- https://doi.org/10.22033/ESGF/CMIP6.10041
  Danabasoglu, G. (2020a). NCAR CESM2-FV2 model output prepared for CMIP6 CMIP AMIP [Dataset]. Earth System Grid Federation. https://
- doi.org/10.22033/ESGF/CMIP6.11287

  Danabasoglu, G. (2020b). NCAR CESM2-WACCM-FV2 model output prepared for CMIP6 CMIP AMIP [Dataset]. Earth System Grid
- Danabasogiu, G. (2020b). NCAR CESM2-WACCM-FV2 model output prepared for CMIP6 CMIP AMIP [Dataset]. Earth System Grid Federation. https://doi.org/10.22033/ESGF/CMIP6.11288
- Dix, M., & Coauthors (2019a). CSIRO-ARCCSS ACCESS-CM2 model output prepared for CMIP6 CMIP historical [Dataset]. Earth System Grid Federation. https://doi.org/10.22033/ESGF/CMIP6.4271
- EC-Earth Consortium (EC-Earth). (2019). EC-Earth-Consortium EC-Earth3-Veg model output prepared for CMIP6 ScenarioMIP [Dataset]. Earth System Grid Federation. https://doi.org/10.22033/ESGF/CMIP6.727
- Guo, H., John, J. G., Blanton, C., McHugh, C., Nikonov, S., Radhakrishnan, A., et al. (2018). NOAA-GFDL GFDL-CM4 model output AMIP [Dataset]. Earth System Grid Federation. https://doi.org/10.22033/ESGF/CMIP6.8494
- Krasting, J. P., John, J. G., Blanton, C., McHugh, C., Nikonov, S., Radhakrishnan, A., et al. (2018). NOAA-GFDL GFDL-ESM4 model output prepared for CMIP6 CMIP AMIP [Dataset]. Earth System Grid Federation. https://doi.org/10.22033/ESGF/CMIP6.8497
- Li, L. (2019). CAS FGOALS-g3 model output prepared for CMIP6 CMIP AMIP [Dataset]. Earth System Grid Federation. https://doi.org/10. 22033/ESGF/CMIP6.3183
- NASA Goddard Institute for Space Studies (NASA/GISS). (2018). NASA-GISS GISS-E2.1G model output prepared for CMIP6 CMIP AMIP [Dataset]. Earth System Grid Federation. https://doi.org/10.22033/ESGF/CMIP6.6984
- NASA Goddard Institute for Space Studies (NASA/GISS). (2019). NASA-GISS GISS-E2-2-G model output prepared for CMIP6 CMIP AMIP [Dataset]. Earth System Grid Federation. https://doi.org/10.22033/ESGF/CMIP6.6986
- Park, S., Shin, J., Kim, S., Oh, E., & Kim, Y. (2019). Global climate simulated by the Seoul National University atmosphere model version 0 with a unified convection scheme (SAM0-UNICON) [Dataset]. *Journal of Climate*, 32(10), 2917–2949. https://doi.org/10.1175/JCLI-D-18-0796.1
- Ridley, J., Menary, M., Kuhlbrodt, T., Andrews, M., & Andrews, T. (2019a). MOHC HadGEM3-GC31-LL model output prepared for CMIP6 CMIP historical [Dataset]. Earth System Grid Federation. https://doi.org/10.22033/ESGF/CMIP6.6109
- Ridley, J., Menary, M., Kuhlbrodt, T., Andrews, M., & Andrews, T. (2019b). MOHC HadGEM3-GC31-MM model output prepared for CMIP6 CMIP AMIP [Dataset]. Earth System Grid Federation. https://doi.org/10.22033/ESGF/CMIP6.5856
- Rong, X. (2019). CAMS CAMS\_CSM1.0 model output prepared for CMIP6 CMIP AMIP [Dataset]. Earth System Grid Federation. https://doi.org/10.22033/ESGF/CMIP6.9712
- Seferian, R. (2018). CNRM-CERFACS CNRM-ESM2-1 model output prepared for CMIP [Dataset]. Earth System Grid Federation. https://doi.org/10.22033/ESGF/CMIP6.1391
- Seland, Ø., Bentsen, M., Oliviè, D. J. L., Toniazzo, T., Gjermundsen, A., Graff, L. S., et al. (2019). NCC NorESM2-LM model output prepared for CMIP6 CMIP AMIP [Dataset]. Earth System Grid Federation. https://doi.org/10.22033/ESGF/CMIP6.7848
- Shiu, C.-J., Lee, W.-L., & Hsu, H.-H. (2021). AS-RCEC TaiESM1.0 model output prepared for CMIP6 CFMIP amip-p4K [Dataset]. Earth System Grid Federation. https://doi.org/10.22033/ESGF/CMIP6.9723
- Song, Z., Qiao, F., Bao, Y., Shu, Q., Song, Y., & Yang, X. (2019). FIO-QLNM FIO-ESM2.0 model output prepared for CMIP6 CMIP historical [Dataset]. Earth System Grid Federation. https://doi.org/10.22033/ESGF/CMIP6.9199
- Tang, Y., Rumbold, S., Ellis, R., Kelley, D., Mulcahy, J., Sellar, A., et al. (2019). MOHC UKESM1.0-LL model output prepared for CMIP 6 CMIP AMIP [Dataset]. Earth System Grid Federation. https://doi.org/10.22033/ESGF/CMIP6.5857
- Tatebe, H., & Watanabe, M. (2018). MIROC MIROC6 model output prepared for CMIP AMIP [Dataset]. Earth System Grid Federation. https://doi.org/10.22033/ESGF/CMIP6.5422

ZHANG ET AL. 9 of 10

- Volodin, E., Mortikov, E., Gritsun, A., Lykossov, V., Galin, V., Diansky, N., et al. (2019). INM INM-CM4-8 model output prepared for CMIP6 CMIP piControl [Dataset]. Earth System Grid Federation. https://doi.org/10.22033/ESGF/CMIP6.5080
- Voldoire, A. (2019a). CNRM-CERFACS CNRM-CM6-1 model output prepared for CMIP6 CFMIP amip-lwoff [Dataset]. Earth System Grid Federation. https://doi.org/10.22033/ESGF/CMIP6.3936
- Voldoire, A. (2019b). CNRM-CERFACS CNRM-CM6-1-HR model output prepared for CMIP6 CMIP AMIP [Dataset]. Earth System Grid Federation. https://doi.org/10.22033/ESGF/CMIP6.3923
- von Storch, J.-S., Putrasahan, D., Lohmann, K., Gutjahr, O., Jungclaus, J., Bittner, M., et al. (2017). MPI-M MPIESM1.2-HR model output prepared for CMIP6 HighResMIP [Dataset]. Earth System Grid Federation. https://doi.org/10.22033/ESGF/CMIP6.762
- Wu, T., Chu, M., Dong, M., Fang, Y., Jie, W., Li, J., et al. (2019). BCC BCC-CSM2MR model output prepared for CMIP6 CMIP AMIP [Dataset]. Earth System Grid Federation. https://doi.org/10.22033/ESGF/CMIP6.2850
- Yu, Y. (2018). CAS FGOALS-f3-L model output prepared for CMIP6 CMIP AMIP [Dataset]. Earth System Grid Federation. https://doi.org/10. 22033/FSGF/CMIP6.3182
- Yukimoto, S., Koshiro, T., Kawai, H., Oshima, N., Yoshida, K., Urakawa, S., et al. (2019). MRI MRI-ESM2.0 model output prepared for CMIP6 CMIP [Dataset]. Earth System Grid Federation. https://doi.org/10.22033/ESGF/CMIP6.621
- Zhang, J., Wu, T., Shi, X., Zhang, F., Li, J., Chu, M., et al. (2019). BCC BCC-ESM1 model output prepared for CMIP6 CMIP AMIP [Dataset]. Earth System Grid Federation. https://doi.org/10.22033/ESGF/CMIP6.2851
- Zhao, M., Golaz, C., Held, I. M., Guo, H., Balaji, V., Benson, R., et al. (2018). NOAA-GFDL GFDL-AM4 model output [Dataset]. Earth System Grid Federation. https://doi.org/10.22033/ESGF/CMIP6.1401
- Ziehn, T., Chamberlain, M., Lenton, A., Law, R., Bodman, R., Dix, M., et al. (2019). CSIRO ACCESS-ESM1.5 model output prepared for CMIP6 CMIP [Dataset]. Earth System Grid Federation. https://doi.org/10.22033/ESGF/CMIP6.2288

ZHANG ET AL. 10 of 10